CHEMISTRY OF MATERIALS
Article

Chem. Mater. **2009,** *21,* 3153–3161 3153
DOI:10.1021/cm900532q

Solution-Processable Barium Titanate and Strontium Titanate Nanoparticle Dielectrics for Low-Voltage Organic Thin-Film Transistors

Qin Jia Cai,[†,§] Ye Gan,[†,§] Mary B Chan-Park,*[†,] Hong Bin Yang,[†] Zhi Song Lu,[†] Chang Ming Li,*[†,] Jun Guo,[‡] and Zhi Li Dong[‡]

[†]*School of Chemical and Biomedical Engineering, Nanyang Technological University, 62 Nanyang Drive, Singapore 637459, and* [‡]*School of Materials Science and Engineering, Nanyang Technological University, Nanyang Avenue, Singapore 639798.* [§]*These authors contributed equally to this work*

Received February 22, 2009. Revised Manuscript Received May 26, 2009

A series of solution-processable oleic-acid capped barium titanate and strontium titanate nanoparticles was synthesized and spin-coated to form homogeneous high-k dielectric films for organic thin-film transistors (TFTs). The dielectric constant k of the nanoparticle films was tunable in the range from 4.1 to 9.3 by altering the molar ratio of oleic-acid surfactant to synthesis precursor. Low-voltage modulated high-performance organic TFTs were fabricated using nanoparticle films as the dielectric components. Flexible bottom-gate pentacene TFTs exhibited outstanding device performance with field-effect mobility, μ, in the range of 2.0−3.5 $cm^2\ V^{-1}\ s^{-1}$ and on/off ratios of about 1×10^4 at low gate voltage. Top-gate poly(3,3‴-didodecylquaterthiophene) TFTs also showed high device performance with μ of 0.05−0.1 $cm^2\ V^{-1}\ s^{-1}$ and on/off ratios of 1×10^3 to 1×10^4. The low-voltage performance of the TFTs could be attributed to a low density of trapped states at the interfaces between the organic semiconductors and the nanoparticle dielectric films. This research provides a series of promising dielectric materials for fabrication of superior organic TFTs through a solution process and fundamentally suggests that low trapped state density at the semiconductor/dielectrics interface may be an important factor to achieve low-voltage modulation in organic TFTs.

Introduction

Printable thin-film transistors (TFTs) are of great interest because of their low cost, light weight, flexibility, and feasibility for large-area coverage and integration.[1−4] The gate dielectric is a key component of the printable TFT and its development has contributed toward the advancement of printable TFTs, such as organic TFTs.[5−13] Silicon dioxide (SiO_2) thin-film thermally grown on silicon (Si) wafer is an excellent dielectric for Si-based transistors and the performance evaluation of organic semiconductors for organic TFTs.[14−17] However, for flexible organic TFTs, solution-processable dielectrics such as polymeric dielectrics are more attractive than SiO_2 because of their low process temperature, mechanical flexibility, and implementability without clean room and vacuum processes.

As the dielectric constant (k) of most polymeric materials is relative low ($k = 2−4$),[5,6] it is often necessary to reduce the film thickness to nanoscale in order to achieve large capacitance. However, polymeric films of nanoscale thickness are problematic because of their structural defects, such as pinholes, which can give rise to excessive gate leakage in organic TFTs.[18,19] To address the gate leakage issue of ultrathin polymer films, researchers have

*Corresponding author. E-mail: mbechan@ntu.edu.sg (M.B.C.-P.); ecmli@ntu.edu.sg (C.M.L).

(1) Javey, A.; Nam; Friedman, R. S.; Yan, H.; Lieber, C. M. *Nano Lett*. **2007**, *7*, 773.
(2) Dimitrakopoulos, C. D.; Malenfant, P. R. L. *Adv. Mater*. **2002**, *14*, 99.
(3) Menard, E.; Meitl, M. A.; Sun, Y. G.; Park, J. U.; Shir, D. J. L.; Nam, Y. S.; Jeon, S.; Rogers, J. A. *Chem. Rev*. **2007**, *107*, 1117.
(4) Yan, H.; Chen, Z.; Zheng, Y.; Newman, C.; Quinn, J. R.; Dotz, F.; Kastler, M.; Facchetti, A. *Nature* **2009**, *457*, 679.
(5) Facchetti, A.; Yoon, M. H.; Marks, T. J. *Adv. Mater*. **2005**, *17*, 1705.
(6) Veres, J.; Ogier, S.; Lloyd, G.; de Leeuw, D. *Chem. Mater*. **2004**, *16*, 4543.
(7) DiBenedetto, S. A.; Frattarelli, D.; Ratner, M. A.; Facchetti, A.; Marks, T. J. *J. Am. Chem. Soc*. **2008**, *130*, 7528.
(8) Chua, L. L.; Zaumseil, J.; Chang, J. F.; Ou, E. C. W.; Ho, P. K. H.; Sirringhaus, H.; Friend, R. H. *Nature* **2005**, *434*, 194.
(9) Halik, M.; Klauk, H.; Zschieschang, U.; Schmid, G.; Dehm, C.; Schutz, M.; Maisch, S.; Effenberger, F.; Brunnbauer, M.; Stellacci, F. *Nature* **2004**, *431*, 963.
(10) Naber, R. C. G.; Tanase, C.; Blom, P. W. M.; Gelinck, G. H.; Marsman, A. W.; Touwslager, F. J.; Setayesh, S.; de Leeuw, D. M. *Nat. Mater*. **2005**, *4*, 243.
(11) Bao, Z. N.; Kuck, V.; Rogers, J. A.; Paczkowski, M. A. *Adv. Funct. Mater*. **2002**, *12*, 526.
(12) Panzer, M. J.; Newman, C. R.; Frisbie, C. D. *Appl. Phys. Lett*. **2005**, *86*, 103503.
(13) Singh Th, B.; Marjanovi, N.; Matt, G. J.; Sariciftci, N. S.; Schwdiauer, R.; Bauer, S. *Appl. Phys. Lett*. **2004**, *85*, 5409.
(14) Fong, H. H.; Pozdin, V. A.; Amassian, A.; Malliaras, G. G.; Smilgies, D.-M.; He, M.; Gasper, S.; Zhang, F.; Sorensen, M. *J. Am. Chem. Soc*. **2008**, *130*, 13202.
(15) Briseno, A. L.; Mannsfeld, S. C. B.; Reese, C.; Hancock, J. M.; Xiong, Y.; Jenekhe, S. A.; Bao, Z.; Xia, Y. *Nano Lett*. **2007**, *7*, 2847.
(16) Gundlach, D. J.; Jia, L. L.; Jackson, T. N. *IEEE Electron. Device Lett*. **2001**, *22*, 571.
(17) Hamadani, B. H.; Corley, D. A.; Ciszek, J. W.; Tour, J. M.; Natelson, D. *Nano Lett*. **2006**, *6*, 1303.
(18) Hwang, D. K.; Lee, K.; Kim, J. H.; Im, S.; Kim, C. S.; Baik, H. K.; Park, J. H.; Kim, E. *Appl. Phys. Lett*. **2006**, *88*, 243513.
(19) Yoon, M. H.; Yan, H.; Facchetti, A.; Marks, T. J. *J. Am. Chem. Soc*. **2005**, *127*, 10388.

Published on Web 06/23/2009

introduced cross-linking agents to produce highly cross-linked ultrathin polymer films, which demonstrate excellent insulating properties and enable low-voltage operation of organic TFTs.[19−23] Because some cross-linking agents are sensitive to humidity, high-quality cross-linked ultrathin polymer films may not be preparable in a common lab under ambient atmosphere.

High-k inorganic materials have been employed as the dielectrics in organic TFTs.[5,6,24−27] A convenient procedure to deposit inorganic gate dielectrics is anodization of metals, which provides attractive "solution-processed" high-quality inorganic oxide dielectrics on gates of suitable metals such as Ti and Ta.[25,26] These inorganic oxide dielectrics showed higher k values than most other common solution-deposited dielectrics and gave rise to low-voltage operation of organic TFTs. Because of their highly hydrophilic surfaces, metal oxide surfaces have been surface-modified by silane or polymers to be compatible with deposition of molecule-ordered semiconductors.[25,27] Recently, atomic-layer-deposited (ALD) HfO_2 combined with spin-cast epoxy has been demonstrated as high-capacitance (up to 330 nF cm^{-2}) bilayer dielectric for low-voltage TFTs in which active component are networks of single-wall carbon nanotubes (SWNTs).[28] The high-capacitance, hysteresis-free, and low-temperature processability of this bilayer dielectric make this process a promising technique for low-voltage organic TFTs in general. Solution processability of inorganic dielectric materials in organic TFTs applications has also been achieved through blending of inorganic nanopowders with polymeric materials to form nanocomposite dielectrics.[29−31] However, the homogeneous distribution of the inorganic nanoparticles in a polymer matrix is still a challenging issue for uniform dielectric properties. An alternative approach is to form high-k inorganic dielectric films via sol−gel processes,[32,33] but this involves relatively high-temperature postdeposition curing treatments (300−700 °C), which is likely to be incompatible with plastic substrates for organic TFTs.

Inorganic colloidal nanoparticles via wet-chemistry have shown promising applications in solar cells,[34] sensors,[35] fuel cells,[36] and biotechnology,[37] as well as nanocomposite dielectrics.[38,39] TiO_2−polystyrene core−shell nanorods synthesized from colloidal TiO_2 nanorods have been solution-processed as high-k dielectrics for organic TFTs.[38] The synthesis procedure for these TiO_2−polystyrene core−shell nanorods is complicated. We have previously demonstrated that homogeneous dielectric film can be obtained from spin-coating with oleic acid stabilized TiO_2 nanoparticles.[40] However, the dielectric constant achieved was still modest (k of about 5.3) and the pentacene based transistors with this dielectric material gave a mobility of about 0.2 $cm^2\ V^{-1}\ s^{-1}$ and an on/off ratio of about 2×10^3. Inorganic colloidal nanoparticles that can be directly solution-processed into high-k inorganic films, without the need for sophisticated nanocomposite synthesis or blending with polymer materials, are urgently needed to fully exploit the simplicity and economic advantages associated with organic TFTs.[40]

In this work, we report the synthesis and application of a series of solution-processable oleic acid (OA) capped barium titanate (OA-$BaTiO_3$) and strontium titanate (OA-$SrTiO_3$) nanoparticles with high dielectric constants ($k = 4.1-9.3$) for low-voltage organic thin-film transistors (TFTs). The as-synthesized nanoparticles were well-dispersed in organic solvent to give clear nanoparticle suspensions, which were directly solution-processed as the dielectric component in organic TFTs by spin-coating on various substrates. The suitability of nanoparticle dielectrics for organic TFTs using pentacene in bottom-gate configuration and poly(3,3‴-didodecylquaterthiophene) in top-gate configuration was also demonstrated. The bottom-gate pentacene TFTs exhibited outstanding device performance with field-effect mobility, μ, in the range of 2.0−3.5 $cm^2\ V^{-1}\ s^{-1}$ and an on/off ratio of about 1×10^4 at low gate voltage. Top-gate Poly(3,3‴-didodecylquaterthiophene) TFTs also showed high device performance with μ of 0.05−0.1 $cm^2\ V^{-1}\ s^{-1}$ and on/off ratios of 1×10^3 to 1×10^4. The organic TFTs showed surprisingly low-voltage driven function and theoretical consideration of the trapped state density at the semiconductor/dielectrics interfaces is suggested to account for the low-voltage function of organic TFTs.

(20) Kim, C.; Wang, Z.; Choi, H.-J.; Ha, Y.-G.; Facchetti, A.; Marks, T. J. *J. Am. Chem. Soc.* **2008**, *130*, 6867.
(21) Jang, Y.; Kim, D. H.; Park, Y. D.; Cho, J. H.; Hwang, M.; Cho, K. W. *Appl. Phys. Lett.* **2006**, *88*, 072101.
(22) Yang, S. Y.; Kim, S. H.; Shin, K.; Jeon, H.; Park, C. E. *Appl. Phys. Lett.* **2006**, *88*, 173507.
(23) Roberts, M. E.; Mannsfeld, S. C. B.; Queraltó, N.; Reese, C.; Locklin, J.; Knoll, W.; Bao, Z. *Proc. Natl. Acad. Sci. U.S.A.* **2008**, *105*, 12134.
(24) Dimitrakopoulos, C. D.; Purushothaman, S.; Kymissis, J.; Callegari, A.; Shaw, J. M. *Science* **1999**, *283*, 822.
(25) Jeong, Y. T.; Dodabalapur, A. *Appl. Phys. Lett.* **2007**, *91*, 193509.
(26) Tate, J.; Rogers, J. A.; Jones, C. D. W.; Vyas, B.; Murphy, D. W.; Li, W.; Bao, Z.; Slusher, R. E.; Dodabalapur, A.; Katz, H. E. *Langmuir* **2000**, *16*, 6054.
(27) Majewski, L. A.; Schroeder, R.; Grell, M. *Adv. Mater.* **2005**, *17*, 192.
(28) Cao, Q.; Xia, M. G.; Shim, M.; Rogers, J. A. *Adv. Funct. Mater.* **2006**, *16*, 2355.
(29) Chen, F. T.; Chu, C. W.; He, J.; Yang, Y.; Lin, J. L. *Appl. Phys. Lett.* **2004**, *85*, 3295.
(30) Schroeder, R.; Majewski, L. A.; Grell, M. *Adv. Mater.* **2005**, *17*, 1535.
(31) Chen, F. C.; Chuang, C. S.; Lin, Y. S.; Kung, L. J.; Chen, T. H.; Shieh, H. P. D. *Org. Electron.* **2006**, *7*, 435.
(32) Anderson, J. T.; Munsee, C. L.; Hung, C. M.; Phung, T. M.; Herman, G. S.; Johnson, D. C.; Wager, J. F.; Keszler, D. A. *Adv. Funct. Mater.* **2007**, *17*, 2117.
(33) Wang, W.; Dong, G.; Wang, L.; Qiu, Y. *Microelectron. Eng.* **2008**, *85*, 414.
(34) Gur, I.; Fromer, N. A.; Geier, M. L.; Alivisatos, A. P. *Science* **2005**, *310*, 462.
(35) Hansen, J. A.; Wang, J.; Kawde, A. N.; Xiang, Y.; Gothelf, K. V.; Collins, G. *J. Am. Chem. Soc.* **2006**, *128*, 2228.
(36) Nam, K. T.; Kim, D. W.; Yoo, P. J.; Chiang, C. Y.; Meethong, N.; Hammond, P. T.; Chiang, Y. M.; Belcher, A. M. *Science* **2006**, *312*, 885.
(37) Bruchez, M.; Moronne, M.; Gin, P.; Weiss, S.; Alivisatos, A. P. *Science* **1998**, *281*, 2013.
(38) Maliakal, A.; Katz, H.; Cotts, P. M.; Subramoney, S.; Mirau, P. *J. Am. Chem. Soc.* **2005**, *127*, 14655.
(39) Jung, C.; Maliakal, A.; Sidorenko, A.; Siegrist, T. *Appl. Phys. Lett.* **2007**, *90*, 062111–3.
(40) Cai, Q. J.; Gan, Y.; Chan-Park, M. B.; Yang, H. B.; Lu, Z. S.; Song, Q. L.; Li, C. M.; Dong, Z. L. *Appl. Phys. Lett.* **2008**, *93*, 113304.

Experimental Section

Materials. Barium oxide (97%), strontium oxide (99.9%), titanium isopropoxide (97%), diphenyl ether (99%), oleic acid (90%), ethylene glycol (99.8%, anhydrous), 2-propanol (99.9%), 30% hydrogen peroxide solution in water, toluene (HPLC), pentacene (99.99%), and ethanol (≥99.8%) were obtained from Sigma-Aldrich and used as received without further purification. Gold (99.999%), silver (99.99%), and titanium (99.995%) pellets for electron beam deposition were obtained from Kurt J. Lesker. Poly(3,3‴-didodecylquaterthiophene) (PQT-12) solution in dichlorobenzene (0.3 wt %) was provided by Xerox Research Centre of Canada.

Synthesis of Barium Titanium Glycolate and Strontium Titanium Glycolate. Barium titanium glycolate and strontium titanium glycolate were synthesized referring to the literature.[41] In a 250 mL round-bottom flask, 78 mmol of barium oxide or strontium oxide fine powder was added into 60 mL ethylene glycol. The reaction mixture was vigorously stirred until the added fine powder was dissolved and then diluted with 80 mL 2-propanol. Titanium isopropoxide (18 mL) was then added into reaction mixture with vigorous stirring for 1 h. The product precipitated from solution was collected by centrifugation, washed with 2-propanol, and dried in a vacuum for further use.

Synthesis of Oleic Acid Capped Barium Titanate and Strontium Titanate. In a 250 mL three-neck flask, a mixture of 50 mL diphenyl ether and 5−45 mmol oleic acid was dried at 120 °C for 1 h under an argon atmosphere with vigorous stirring. After the mixture was cooled to 100 °C, 5 mmol barium titanate glycolate or strontium titanate glycolate was added to the mixture under vigorous stirring until the added precursors was dissolved. 1.8 g 30% hydrogen peroxide in water was then injected into the mixture slowly (vigorous exothermic reaction). The mixture was maintained in a closed system at 100 °C and stirred under a mild reflux with water for 48 h in an inverse micelle condition. After the reaction mixture was cooled to room temperature, the product was readily precipitated upon addition of an excess of ethanol to the reaction mixture. The resulting precipitate was isolated by centrifugation and repeatedly washed with ethanol to remove the surfactant residuals. The ethanol-wetted precipitate was dispersed into toluene with assistance of sonication. By low-speed centrifugation (5000 rpm) for 5 min, nondispersed precipitate was isolated from the suspension to give clear light-yellow suspensions of OA-capped nanoparticles, which were stored at room temperature for characterizations and device fabrication.

Material Characterizations. Transmission electron microscopy (TEM) images were obtained using a JEOL JEM-2100F transmission electron microscope operating at 200 kV. The samples were prepared by dropping the dilute nanoparticles suspensions in toluene onto 300 mesh copper grids and evaporating the solvent. Attenuated total reflectance Fourier transform infrared (ATR-FTIR) spectra were collected using a Thermo Nicolet 5700 FT-IR spectrometer with a resolution of 1 cm^{-1}. AFM experiments were conducted with a Nanoscope IIIa MultiMode scanning probe microscope (Digital Instruments) in tapping mode with a scan rate of 0.5 Hz.

Device Fabrication and Characterizations. (1) Capacitors: Indium tin oxide (ITO) glass substrates were cleaned with methanol, acetone, and isopropanol assisted with sonication, and subsequently treated with oxygen plasma for 2 min. OA-capped nanoparticle suspensions in toluene (~40 mg/g) were spin-coated on treated ITO substrates under 500−600 rpm for 45 s and silver top contacts of about 100 nm thickness and 4 mm^2 in area were deposited on the nanoparticle films under 1×10^{-7} torr. (2) Bottom-gate pentacene TFTs: Bottom-gate pentacene TFTs were fabricated on ITO/PET or Al/SiO_2 substrates. OA-capped nanoparticle suspensions in toluene (~40 mg/g) were spin-coated to deposit nanoparticle dielectric films on ITO/PET or Al/SiO_2 substrates. Pentacene films of about 35 nm were deposited on the nanoparticle films with a rate of 5 nm/min and Au source-drain electrodes of 100 nm were deposited via a shadow mask. In addition, bottom-gate pentacene devices were also fabricated on heavily doped n-type silicon wafer with 100 nm top-layer of SiO_2 as insulator. The SiO_2 surfaces were treated with 10 mmol octyltrichlorosilane (OTS) solution in hexane for 20 min before pentacene deposition. (3) Top-gate PQT-12 TFTs: Top-gate PQT-12 TFTs were fabricated on oxide Si wafers with gold/titanium (Au/Ti: 50 nm/1 nm) source-drain contacts patterned using lift-off technique. The Au contacts and oxide Si surfaces were treated with Piranha solution briefly and octyltrichlorosilane (OTS-8) solution, respectively. PQT-12 semiconductor layers of about 60 nm were deposited on the substrates, annealed at 125 °C for 30 min and cooled to room temperature overnight in a vacuum. OA-capped nanoparticle suspensions in toluene (~40 mg/g) were subsequently spin-coated on the PQT-12 semiconductor layers subsequently to deposit nanoparticle dielectric films. Finally, silver top-gates of about 100 nm thickness were deposited on the nanoparticle dielectric films under about 1×10^{-7} torr. (4) device characterizations: The capacitors were characterized using an HP 4284 Precision LCR meter. The dielectric constant was determined from capacitance measurement using the relationship: $C_i = \varepsilon_0 k/d$ (ε_0 is the permittivity of vacuum, k is the dielectric constant, and d is the thickness). The organic TFTs were characterized using an Agilent 4157B Semiconductor Parameter Analyzer System. Device mobilities in the saturation regimes were extracted from the following equations: $I_D = C_i\mu(V_G - V_{th})^2 W/2L$, where I_D is the drain current, C_i is the capacitance per unit area of the gate dielectric layer, and V_G and V_{th} are gate and threshold voltage.

Results and Discussion

Images a and b in Figure 1, respectively, show the digital photographs of a series of dispersions of OA-$BaTiO_3$ and OA-$SrTiO_3$ nanoparticles, which were synthesized with [OA]/[P] (P, precursor) molar ratios ranging from 1 to 9. For all [OA]/[P] ratios, the as-synthesized nanoparticles of different [OA]/[P] ratio were well-dispersed in toluene, giving clear nanoparticle suspensions. As shown respectively in images a and b in Figure 1, the OA-$BaTiO_3$ and OA-$SrTiO_3$ suspensions darken from left to right with increasing [OA]/[P] ratio, which is expected because the number of particles per unit volume of suspension increases with that ratio. The nanoparticle suspensions have been stable for more than 9 months, with negligible precipitation at the time of this writing. Images c and d in Figure 1 transmission electron microscopy (TEM) images of representative OA-$BaTiO_3$ and OA-$SrTiO_3$ nanoparticles of [OA]/[P] =1 with sizes of 3−5 nm and high-resolution TEM lattice images of single OA-$BaTiO_3$ and OA-$SrTiO_3$ nanoparticles of [OA]/[P] = 1 (insets to c and d in Figure 1). As the [OA]/[P] ratio

(41) Day, V. W.; Eberspacher, T. A.; Frey, M. H.; Klemperer, W. G.; Liang, S.; Payne, D. A. *Chem. Mater.* **1996**, *8*, 330.

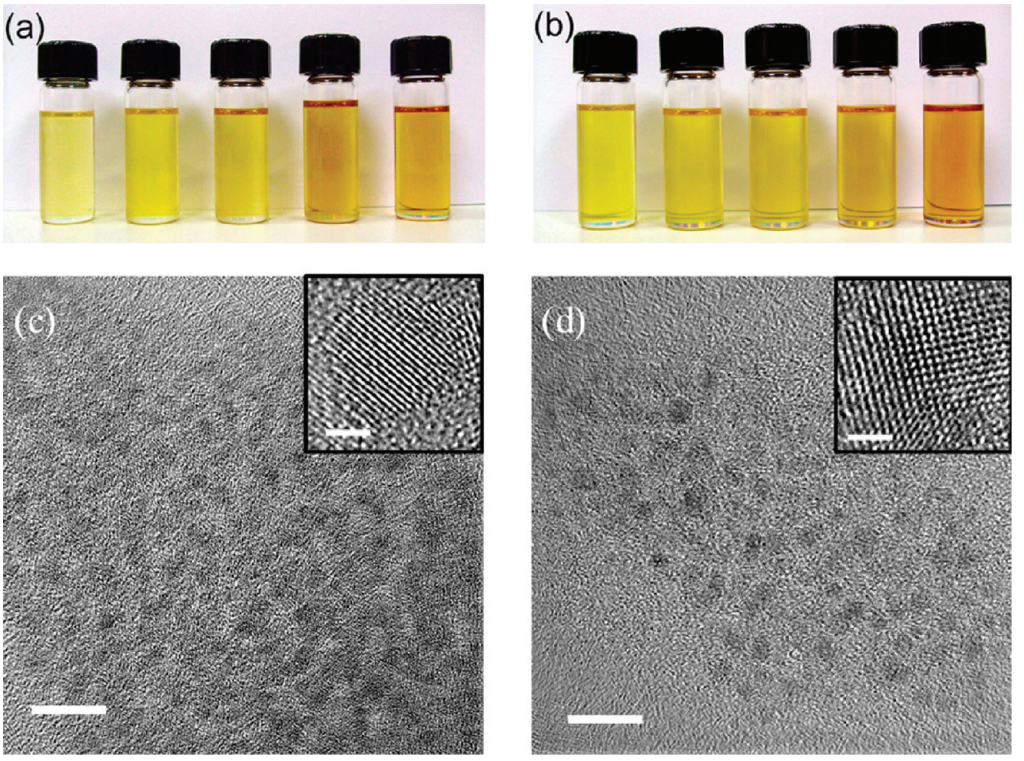

Figure 1. Digital images of clear (a) OA-$BaTIO_3$ and (b) OA-$SrTiO_3$ nanoparticle suspensions in toluene (~40 mg/g) and representative TEM images of (c) OA-$BaTIO_3$ ([OA]/[P] = 1) and (d) OA-$SrTiO_3$ ([OA]/[P] = 1) nanoparticles. The c and d scale bars are 10 nm. From left to right in a and b, the nanoparticles formulations are [OA]/[P] = 1, 2, 3, 5, and 9. The insets in c and (d) are high-resolution TEM images of a representative single OA-$BaTiO_3$ and OA-$SrTiO_3$ nanoparticles, respectively. The inset scale bars are 2 nm.

increased to 9, the nanoparticle size decreased gradually to 2−3 nm.

The organic surfactant, OA, is critical for good dispersion of the inorganic nanoparticles in organic solvent. The surface immobilization of OA onto inorganic core nanoparticle surfaces was confirmed with Fourier transform infrared (FT-IR) spectroscopy. Figure 2 presents representative FT-IR spectra of OA-$BaTiO_3$ and OA-$SrTiO_3$ nanoparticles and a comparison spectrum of OA. Both OA-capped nanoparticles samples (spectra a and b in Figure 2) and the OA sample (Figure 2c) exhibit strong absorption peaks at 2923 and 2853 cm^{-1}, which are due to the intense antisymmetric and symmetric C−H stretching vibrations of the $-CH_2-$ groups, respectively.[42] A weak absorption band at 3010 cm^{-1}, attributable to the olefinic C−H stretching vibration,[42] is also observable in Figure 2a−c. It suggested that the carbon−carbon double bond in OA could be preserved during nanoparticle synthesis, although cross-linking or polymerization of OA cannot be ruled out. The free C=O stretching vibration leads to a strong absorption peak at 1709 cm^{-1} in the OA spectrum (Figure 2c).[42] This feature is absent from the spectra of OA-capped nanoparticles (spectra a and b in Figure 2). In contrast, two characteristic absorption peaks at 1545 and 1403 cm^{-1} are apparent in the nanoparticle spectra (spectra a and b in Figure 2) that are due to the COO^- antisymmetric and symmetric stretching

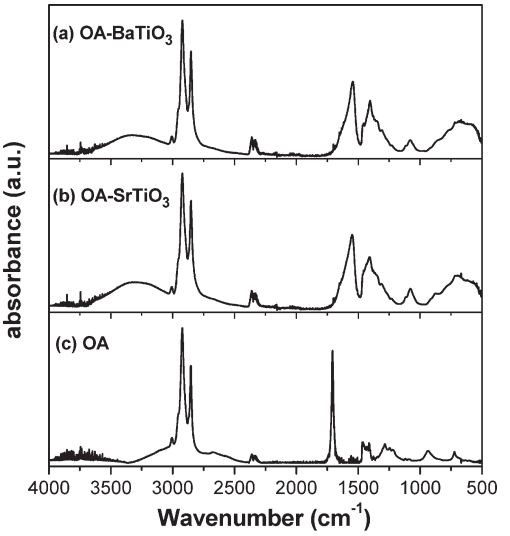

Figure 2. FT-IR spectra of representative (a) OA-$BaTiO_3$ ([OA]/[P] = 1), (b) OA-$SrTiO_3$ ([OA]/[P] = 1) nanoparticles, and (c) oleic-acid (OA).

vibrations, respectively, of carboxylate anions complexed with surface metal centers of the nanoparticles.[43,44] The frequency difference ($\Delta\nu \approx 142$ cm^{-1}) between the two absorption bands suggests that the binding mode of carboxylate on the inorganic core nanoparticle surfaces may be in the chelating bidentate form.[45] These results suggest that the stabilizing OA ligands are effectively

(42) Pretsch, E., Bühlmann, P., Affolter, C. Structure Determination of Organic Compounds−Tables of Spectral Data, 3rd ed.; Springer-Verlag: New York, 2003.

(43) Thistlethwaite, P. J.; Hook, M. S. *Langmuir* **2000**, *16*, 4993.
(44) Cozzoli, P. D.; Kornowski, A.; Weller, H. *J. Am. Chem. Soc.* **2003**, *125*, 14539.
(45) Nara, M.; Torii, H.; Tasumi, M. *J. Phys. Chem.* **1996**, *100*, 19812.

bonded to the surfaces of the inorganic core nanoparticles and that free OA is nearly absent in the nanoparticles suspensions.

Given the excellent dispersion of OA-$BaTiO_3$ and OA-$SrTiO_3$ nanoparticles in toluene, homogeneous and transparent nanoparticle films (280−350 nm in thickness) were easily deposited, via spin-coating under ambient condition, on indium tin oxide (ITO)-coated glass, ITO-coated polyethylene terephthalate (PET), and silicon wafers substrates. The spin-coated films were dried under a vacuum at room temperature. The surfaces of the resulting nanoparticle films were smooth. As shown in Figure 3, films made with OA-$BaTiO_3$ and $SrTiO_3$ nanoparticles formulated with [OA]/[P] = 1 had root-mean-square roughness (R_{rms}) values of about 7 nm over a 25 μm^2 area, determined with atomic force microscopy (AFM). Films made with nanoparticles of higher [OA]/[P] molar ratios showed reduced surface roughness, with R_{rms} values in the range of 0.5−4 nm. In addition, the resulting film surfaces are characteristics of low surface energy with water contact angles of 95−103°.

To evaluate their dielectric properties, we sandwiched homogeneous OA-$BaTiO_3$ and OA-$SrTiO_3$ nanoparticle films between ITO-coated glass substrates (bottom-electrodes) and vacuum-deposited aluminum (Al) films (top-electrodes) to form capacitors. Figure 4 shows plots of the dielectric constant and inorganic volume fraction vs [OA]/[P] molar ratio for these films. For the lowest molar ratio nanoparticle formulation, [OA]/[P] = 1, the OA-$BaTiO_3$ and OA-$SrTiO_3$ films exhibited dielectric constants of 9.3 and 7.1, respectively, which are 4- and 3-times that of bulk OA ($k = 2.3$).[46] The inorganic $BaTiO_3$ and $SrTiO_3$ volume fractions were estimated to be 0.16 and 0.18 for OA-$BaTiO_3$ and OA-$SrTiO_3$ nanoparticles with [OA]/[P] = 1, respectively. When the [OA]/[P] ratio was increased in the synthesis, the inorganic $BaTiO_3$ and $SrTiO_3$ volume fractions decreased gradually to about 0.14 and 0.09 at [OA]/[P] = 9, respectively. The decrease in inorganic volume fraction with increased [OA]/[P] ratio is probably due to the fact that the size of the synthesized inorganic cores decreased with increased [OA]/[P] ratio, which have previously been used to controlled the size of inorganic nanoparticles in nanoparticle synthesis.[47,48] As the [OA]/[P] molar ratio increased from 1 to 9, the k values of OA-$BaTiO_3$ and OA-$SrTiO_3$ nanoparticle films decreased significantly, from 9.3 to 4.1 and 7.1 to 4.5, respectively. The trend of k variation with [OA]/[P] molar ratio is consistent with the inorganic volume fraction variation. This phenomenon is consistent with other reports of nanocomposite materials,[38,39] for which k decreased as the volume fraction of the inorganic component decreased. On the other hand, the OA-$BaTiO_3$ and OA-$SrTiO_3$ dielectric films (except for the OA-$BaTiO_3$ film with [OA]/[P] = 9) exhibited good insulating properties with low leakage current densities and reasonable electrical strength. As shown in panels a and b in Figure 5, the as-spin-coated nanoparticle films generally gave electric current densities of 1×10^{-5} to 1×10^{-7} A/cm^2 at electric fields in the range of 0.5−1 MV/cm, and electrical strength > 1 MV/cm. The single exception to this was the $BaTiO_3$ nanoparticle film with [OA]/[P] = 9, which had a relatively low electrical strength, ≤ 0.3 MV/cm.

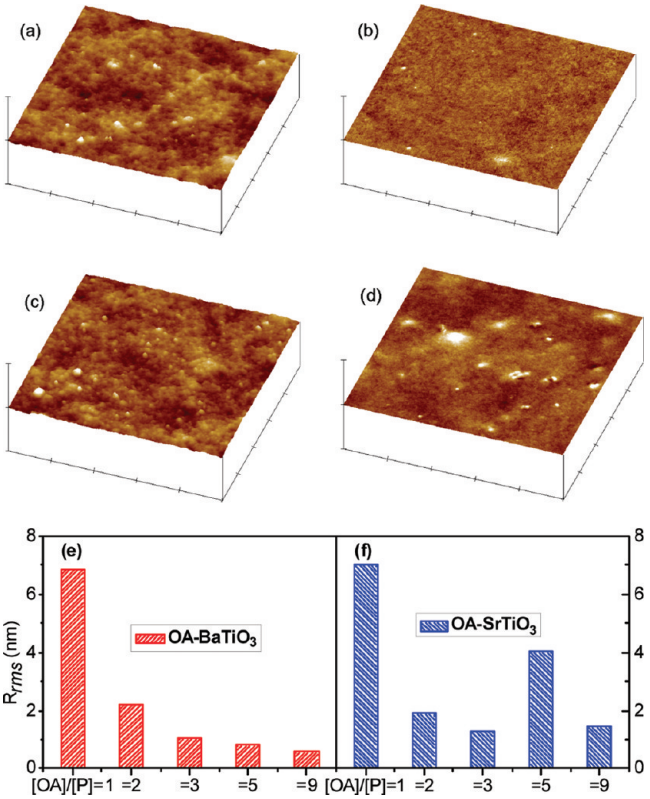

Figure 3. Atomic force microscopy (AFM) images of (a) OA-$BaTiO_3$ of [OA]/[P] = 1, (b) OA-$BaTiO_3$ of [OA]/[P] = 3, (c) OA-$SrTiO_3$ of [OA]/[P] = 1, and (d) OA-$SrTiO_3$ of [OA]/[P] = 9 thin films spin-coated on silicon substrates. The X, Y, and Z scales are 5, 5, and 0.5 μm. (e, f) R_{rms} vs [OA]/[P] plots for OA-$BaTiO_3$ and OA-$SrTiO_3$ films, respectively.

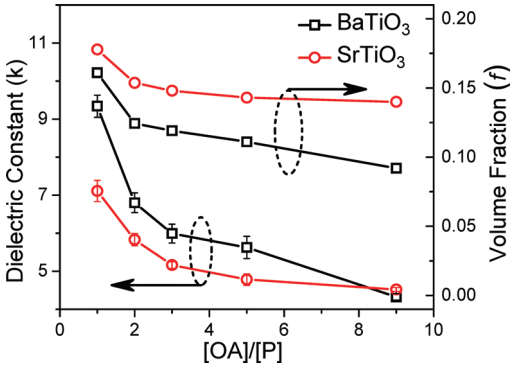

Figure 4. Dielectric constant (k) and inorganic volume fraction (f) vs [OA]/[P] molar ratio plots. The k values were determined at frequency of 100 Hz. Inorganic volume fraction estimation: dry OA-capped nanoparticles were annealed under 500 °C and nitrogen gas for 30 min and the inorganic residue was determined to have a weight fraction. Assuming the densities of pure $BaTiO_3$, $SrTiO_3$, and OA to be 6.08, 4.81, and 0.89 g/cm^2, respectively, we estimated the inorganic volume fraction of each OA-capped nanoparticles.

(46) Lide, D. R. CRC Handbook of Chemistry and Physics, 85th ed.; CRC Press: Boca Raton, FL, 2005; pp 6−175.
(47) O'Brien, S.; Brus, L.; Murray, C. B. *J. Am. Chem. Soc.* **2001**, *123*, 12085.
(48) Cozzoli, P. D.; Kornowski, A.; Weller, H. *J. Am. Chem. Soc.* **2003**, *125*, 14539.

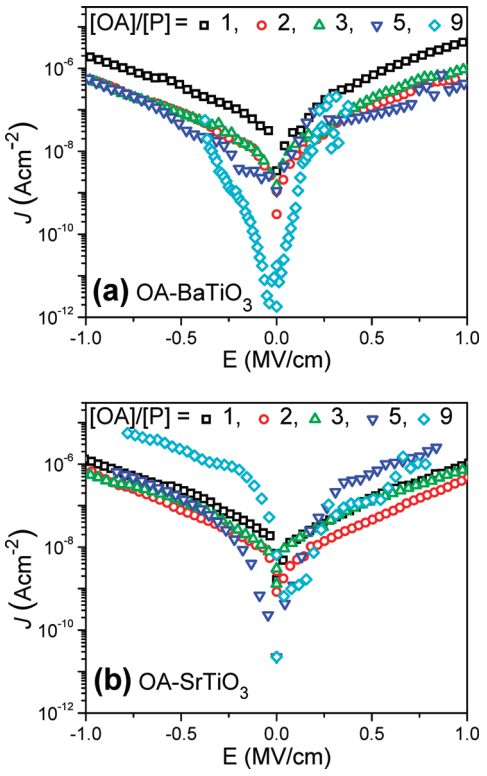

Figure 5. Current densities vs electric field plots of (a) OA-$BaTiO_3$ and (b) OA-$SrTiO_3$ nanoparticle dielectric films.

Bottom- and top-gate organic TFTs were fabricated with nanoparticle dielectric thin films ($k \geq 5$) to assess the utility of these materials as device components. The device geometries are illustrated in panels a and b in Figure 6. Panels b and d in Figure 7 show representative transfer characteristics and $(I_D)^{1/2}$ vs V_G plots of bottom-gate pentacene TFTs with OA-$BaTiO_3$ and OA-$SrTiO_3$ dielectrics. The OA-$BaTiO_3$ thin film of approximately 330 nm in thickness was made with the [OA]/[P] = 1 formulation ($k \approx 9.3$) and the OA-$SrTiO_3$ thin film of approximately 340 nm was made with the [OA]/[P] = 2 formulation ($k \approx 5.9$). As shown in Figure 7b, the pentacene TFTs with OA-$BaTiO_3$ dielectrics on the PET substrates exhibited a field-effect mobility of about 3.5 $cm^2\ V^{-1}\ s^{-1}$, with on/off ratio of about 2×10^4 under low operating voltages of $V_D = V_G = -2$ V. The subthreshold swing (S) of the device was about 106 mV/dec With OA-$SrTiO_3$ dielectrics, the bottom-gate pentacene device in Figure 7d was operated with higher voltages of $V_D = V_G = -10$ V. It gave field-effect mobility of about 3.0 $cm^2\ V^{-1}\ s^{-1}$ and on/off ratios of about 2×10^4 with a subthreshold swing of about 517 mV/dec. The pentacene TFTs with the selected OA-$BaTiO_3$ and OA-$SrTiO_3$ dielectrics on plastic substrates typically showed field-effect mobilities of 2.0−3.5 $cm^2\ V^{-1}\ s^{-1}$ under operating voltages of $|V_D| = |V_G| \leq 10$ V.

For comparison, pentacene TFTs were fabricated with the same device configuration, but using 100 nm SiO_2 dielectrics on heavily doped n-type Si wafers. The SiO_2 surfaces were pretreated with octyltrichlorosilane (OTS). Similar to the OA-capped nanoparticle film, OTS-treated SiO_2 (OTS-SiO_2) surfaces have low surface energy (water contact angle of ~98°) and alkyl-chains at the topmost

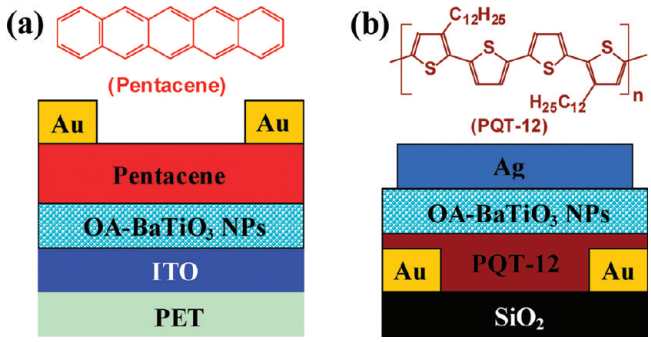

Figure 6. Schematic illustrations of (a) bottom-gate and (b) top-gate organic TFT device configurations for organic TFTs.

surfaces, which may induce similar molecular arrangement and orientation of vapor-deposited pentacene on the respective substrates.[49] The pentacene devices with OTS-SiO_2 dielectrics showed an average field-effect mobility of only ~0.38 $cm^2\ V^{-1}\ s^{-1}$ with an on/off ratio of about 1×10^3 under drain and gate voltages of 35 V (see the Supporting Information, Figure S5). The pentacene/OA-$BaTiO_3$ TFT in Figure 7b had performance metrics much superior to those of the comparison device using OTS-SiO_2 dielectrics. Compared to the pentacene/OTs-SiO_2 device, The pentacene/OA-$BaTiO_3$ device had almost one-order of magnitude higher field-effect mobility, and this was obtained under operating conditions of more than one-order of magnitude lower gate-field (E) and charge per unit area (Q_S) at the semiconductor/dielectrics interface. It is also notable that the pentacene/OA-$BaTiO_3$ TFTs showed low-voltage function with high device performance as those organic TFTs did with ultrathin (< 50 nm) cross-linked polymer or polymer blends dielectrics,[19−23] despite the much lower capacitance values (15−25 nF cm^{-2}) of the nanoparticle dielectric films than those (200−400 nF cm^{-2}) of ultrathin cross-linked polymer or polymer blend dielectrics.[19−23] Figure 8 shows the surface morphology of pentacene on OA-$BaTiO_3$ surface and OTS-SiO_2 surface. The pentacene crystalline grains are smaller on OA-$BaTiO_3$ than on OTS-SiO_2. The formation of larger grains in a bulk film, with the attendant lower areal density of grain boundaries, may benefit the charge transport in semiconductor films.[2] The AFM results suggests that the higher device performance on OA-$BaTiO_3$ dielectric than on OTS-SiO_2 dielectric may not be due to the morphology of the pentacene thin films.

These phenomena can be understood through consideration of the trapped state density at semiconductor/dielectric interfaces in a trapping model,[50] which has been successfully applied to describe pentacene-based TFT behaviors.[24,51,52] This model assumes that there is a large density of trapped states (localized states) in the

(49) Knipp, D.; Street, R. A.; Volkel, A.; Ho, J. *J. Appl. Phys.* **2003**, *93*, 347.
(50) Le Comber, P. G.; Spear, W. E. *Phys. Rev. Lett.* **1970**, *25*, 509.
(51) Street, R. A.; Knipp, D.; Volkel, A. R. *Appl. Phys. Lett.* **2002**, *80*, 1658.
(52) Pernstich, K. P.; Haas, S.; Oberhoff, D.; Goldmann, C.; Gundlach, D. J.; Batlogg, B.; Rashid, A. N.; Schitter, G. *J. Appl. Phys.* **2004**, *96*, 6431.

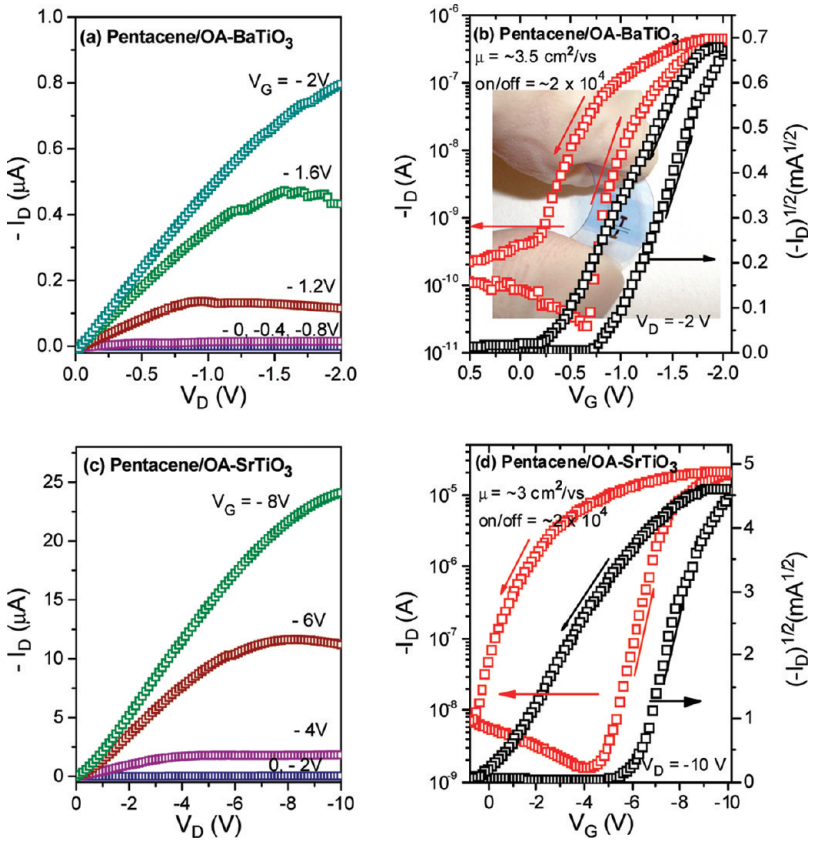

Figure 7. Output characteristics, transfer characteristics, and $(I_D)^{1/2}$ vs V_G plots of bottom-gate pentacene TFTs based on (a, b) OA-$BaTiO_3$ ([OA]/[P]=1, k=9.3, and channel width/length (W/L=13) and (c, d) OA-$SrTiO_3$ ([OA]/[P]=2, k=5.9, and W/L=45) nanoparticle dielectrics. The sweep rates in transfer characteristics are 0.55 and 0.45 V/s for pentacene/OA-$BaTiO_3$ and pentacene/ OA-$SrTiO_3$ devices, respectively. The background image in b is a photograph of the pentacene TFTs with OA-$BaTiO_3$ dielectric demonstrating its mechanical flexibility.

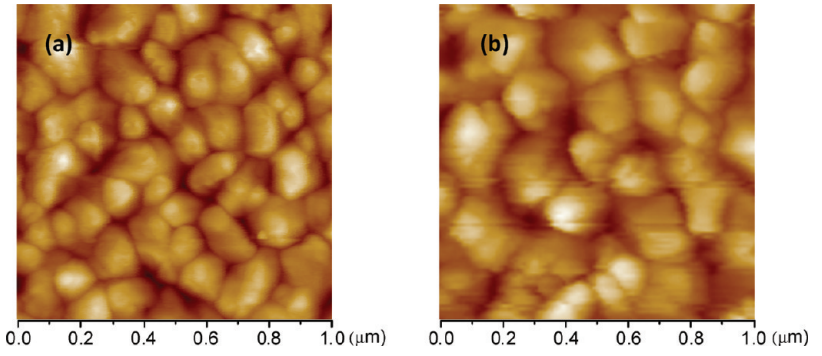

Figure 8. AFM images of pentacene films of 35 nm deposited on (a) OA-$BaTiO_3$ and (b) OTS-SiO_2 substrates.

forbidden band gap of the semiconductors. As gate voltage increases, the deepest trapped states are filled first as the Fermi level approaches the delocalized band edge (such as the highest occupied molecular orbital (HOMO) in pentacene). The threshold voltage is reached when all deep trapped states are filled and the local Fermi level overlaps the energy level that thermally activated carriers can occupy. This condition could be described as the equilibrium state between trapped and mobile carriers. If all the trapped states are filled at a higher voltage, any subsequently injected carriers are free to move in the delocalized band and the field-effect mobility is independent of the gate voltage. According to this model, it is expected that a higher concentration of trapped states in the gap would require a larger number of compensating charge carriers to be injected under higher gate voltage.

It is known that the trapped states at semiconductor/dielectric interface are attributable to interface chemical defects, such as Si−OH species, which can influence the charge transport by trapping/scattering charge carriers at the interfaces.[8,53,54] These trapped states are critical for organic transistors, since the charge transport channel is believed to be within the several semiconductor monolayers adjacent to the dielectric surfaces. The trapped

(53) McDowell, M.; Hill, I. G.; McDermott, J. E.; Bernasek, S. L.; Schwartz, J. *Appl. Phys. Lett.* **2006**, *88*, 073505.
(54) Yoon, M. H.; Kim, C.; Facchetti, A.; Marks, T. J. *J. Am. Chem. Soc.* **2006**, *128*, 12851.

Table 1. Field-Effect Mobility μ, Threshold Voltage V_{th}, Turn-On Voltage V_{on}, and Estimated Trapped State density N_{trap} of Bottom-Gate Pentacene and Top-Gate PQT-12 TFTs, As Well As Bottom-Gated Pentacene TFTs with 100 nm OTS-SiO_2 on n^{++}Si Substrates for Comparison[a]

device	interface	μ ($cm^2V^{-1}s^{-1}$)	C ($nFcm^{-2}$)	V_{th} (V)	V_{on} (V)	N_{trap} ($\times 10^{11}cm^{-2}$)
bottom-gate pentacene TFTs	pentacene/OTS-SiO_2	~0.38	34	−13.5	−7.2	13.4
	pentacene/OA-$BaTiO_3$	~3.5	25	−0.87	−0.65	0.34
	pentacene/OA-$SrTiO_3$	~3.0	15.4	−6.12	−4.91	1.16
top-gate PQT-12 TFTs	PQT-12/OA-$BaTiO_3$	~0.06	21	0.23	0.92	0.90
	PQT-12/OA-$SrTiO_3$	~0.1	20	0.32	0.59	0.46

[a] N_{trap} was estimated using the relationship of $N_{trap} = C_{in}|V_{on} - V_{th}|/q$.[52,53] V_{th} was determined by extrapolating the fitting line for $(I_D)^{1/2}$ vs V_G to zero current. V_{on}, the voltage at which subthreshold current starts increasing exponentially, was extracted from the I_D vs V_G characteristic plotted on a semi-logarithmic scale.

state density can be estimated with the relation:[52,53] $N_{trap} = C_{in}|V_{on} - V_{th}|/q$, where N_{trap} is the trapped state densities, C_{in} is insulator capacitance per unit area, V_{on} and V_{th} are turn-on voltage and threshold voltage, and q is the electron charge. Table 1 lists the estimated trapped state density for TFTs with the semiconductor/dielectrics interfaces studied in this report. The pentacene TFTs with OTS-SiO_2 dielectrics had a trapped state density of about $1.34 \times 10^{12}/cm^2$, which is consistent with values for octadecyltrichlorosilane-treated SiO_2 dielectrics reported in the literatures.[52] For the pentacene device with OA-$BaTiO_3$ (Figure 7b), the trapped state density is estimated to be $3.4 \times 10^{10}/cm^2$, nearly 40 times lower than that of TFTs with OTS-SiO_2. Much lower (>10-fold) trapped state density ($1.16 \times 10^{11}/cm^2$) was also estimated for the device with OA-$SrTiO_3$ dielectric (Figure 7c). Another model ($N_{trap}{}^{max} \approx C_{in}[qS\log(e)/k_BT - 1]/q$,[43,54] where $N_{trap}{}^{max}$ is maximum trapped state density, S is subthreshold swing, k_B and T are Boltzmann's constant and temperature, and e is the base of the natural logarithms) leads to similar inferences that the devices with OA-$BaTiO_3$ and OA-$SrTiO_3$ dielectrics in panels b and d in Figure 7 have trapped state densities more than one-order of magnitude lower than that of devices with OTS-SiO_2 dielectrics. Because low trapped state density requires less compensating charge carrier injection, it is reasonable that the pentacene TFTs with nanoparticle dielectrics could be operated under low gate voltage with high device performance. These results suggest that OA-$BaTiO_3$ and OA-$SrTiO_3$ dielectrics may match pentacene films to form excellent semiconductor/dielectric interfaces with low trapped state density.

Low-voltage TFTs were also demonstrated in top-gate poly(3,3‴-didodecylquaterthiophene) (PQT-12) with OA-$BaTiO_3$ (~290 nm, [OA]/[P] = 2, $k \approx 6.8$) and OA-$SrTiO_3$ (~330 nm, [OA]/[P] = 1, $k \approx 7.1$) nanoparticle dielectrics. The device configuration is illustrated in Figure 6b. The dielectric layers were spin-coated on PQT-12 films under ambient conditions. Panels b and d in Figure 9 are representative transfer characteristics and $(I_D)^{1/2}$ vs V_G plots of the top-gate PQT-12 TFTs. The devices gave a field-effect mobility of ~0.06 and an on/off ratio of about 1×10^4 for OA-$BaTiO_3$ and a mobility of ~0.1 $cm^2\,V^{-1}\,s^{-1}$ and an on/off ratio of about 1×10^3 for OA-$SrTiO_3$ under low-voltage operation ($V_D = V_G = -3$ V) and current modulation of more than 1×10^3 for gate voltage variations of about 4 V. Low trapped state density values ($< 1 \times 10^{11}/cm^2$, Table 1) are also suggested for these PQT-12 TFTs. These results suggest that these high-k nanoparticle dielectrics may result in low trapped state densities at semiconductor/dielectrics interfaces, which account for the low-voltage function and high performance of the organic TFTs.

Hysteresis and its dependence on sweep rate are well-known in most organic TFTs. Figures 7b, 7d, 9b, and 9d show the transfer characteristics of devices using OA-capped nanoparticle dielectrics with forward (positive to negative) and reverse (negative to positive) sweeps. Considerable hysteresis is observed for pentacene and PQT-12 TFTs based on OA-capped nanoparticle dielectrics with sweep rates in the range of 0.45−0.90 V/s. The hysteresis is probably associated with the trapping of electron injected from the gate.[55,56] As shown in Figure 10, the hysteresis for TFTs with OA-capped nanoparticle dielectric was substantially suppressed by slowing the sweep rate from 0.45 to 0.08 V/s. Hysteresis has been widely observed in organic TFTs using polymeric high-k dielectric materials, such as poly(vinyl alcohol),[57] poly(4-vinyl phenol),[58] polymer electrolyte (polyethylene oxide containing $LiClO_4 \cdot 3H_2O$),[12] as well as sol−gel silica dielectrics.[59] The trapping of injected electrons from the gate and insufficient ion migration velocity account for the hysteresis of these dielectrics. For polymer electrolyte and sol−gel silica dielectrics, a sweep rate of about 0.01 V/s was necessary to suppress or eliminate the hysteresis behaviors.[12,59] Much reduced hysteresis has been demonstrated in pentacene TFTs with inorganic oxide dielectric from anodization of Ta (Ta_2O_5) and Ti (TiO_2).[25,60] The device mobilities of these low-voltage pentacene TFTs were less than 1 $cm^2\,V^{-1}\,s^{-1}$, although these dielectric surfaces had been treated by a silane to reduce the surface trapping centers for charge carriers.

(55) Huang, C.; West, J. E.; Katz, H. E. *Adv. Funct. Mater.* **2007**, *17*, 142.
(56) Hwang, D. K.; Oh, M. S.; Hwang, J. M.; Kim, J. H.; Im, S. *Appl. Phys. Lett.* **2008**, *92*, 013304.
(57) Lee, C. A.; Park, D. W.; Jin, S. H.; Park, I. H.; Lee, J. D.; Park, B. G. *Appl. Phys. Lett.* **2006**, *88*, 252102.
(58) Lee, C. A.; Park, D. W.; Jung, K. D.; Kim, B. J.; Kim, Y. C.; Lee, J. D.; Park, B. G. *Appl. Phys. Lett.* **2006**, *89*, 262120.
(59) Cahyadi, T.; Tan, H. S.; Mhaisalkar, S. G.; Lee, P. S.; Boey, F.; Chen, Z. K.; Ng, C. M.; Rao, V. R.; Qi, G. J. *Appl. Phys. Lett.* **2007**, *91*(24), 242107.
(60) Majewski, L. A.; Schroeder, R.; Grell, M. *Adv. Funct. Mater.* **2005**, *15*, 1017.

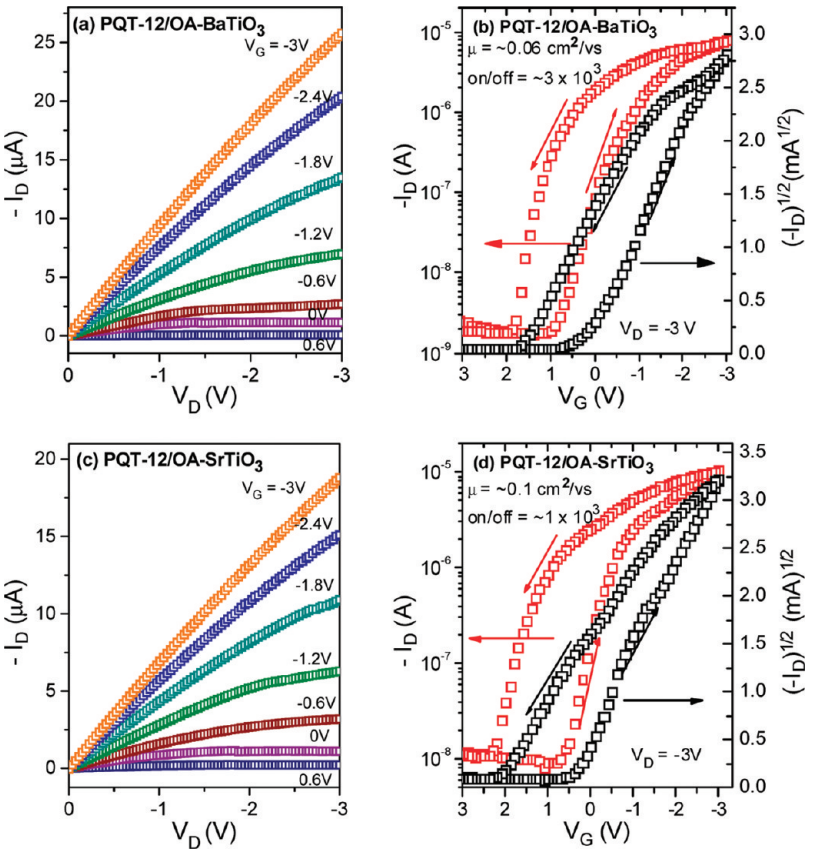

Figure 9. Output characteristics, transfer characteristics, and $(I_D)^{1/2}$ vs V_G plots of top-gate PQT-12 TFTs with (a, b) OA-$BaTiO_3$ ([OA]/[P] = 2, k = 6.8, and W/L = 1800) and (c, d) OA-$SrTiO_3$ ([OA]/[P] = 1, k = 7.1 and W/L = 1800) nanoparticle dielectrics. The sweep rate in transfer characteristics are 0.75 and 0.90 V/s for PQT-12/ OA-$BaTiO_3$ and PQT-12/ OA-$SrTiO_3$ devices, respectively.

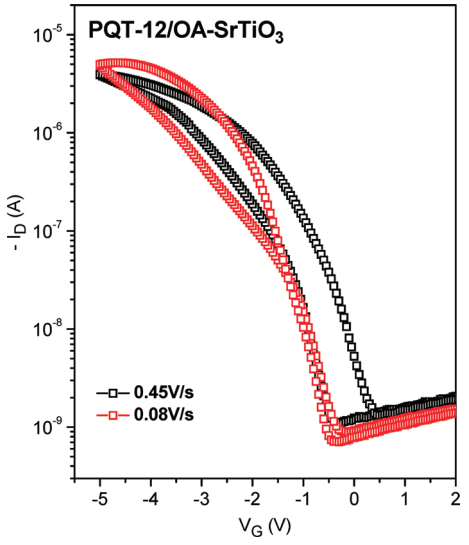

Figure 10. Reduction of sweep rate significantly reduces hysteresis of a PQT-12 based TFT with OA-capped nanoparticle dielectric.

Summary

In summary, a series of soluble OA-$BaTiO_3$ and OA-$SrTiO_3$ nanoparticles were synthesized and applied as dielectrics in low-voltage organic TFTs. The nanoparticles were well-dispersed in organic solvent, which facilitates low-temperature solution-phase processing and fabrications of low-cost flexible organic TFTs on plastic substrates. High-performance, low-voltage organic TFTs in bottom- and top-gate device configurations were demonstrated using high-k nanoparticle films as dielectric layers. Pentacene TFTs had mobilities of 2.0−3.5 $cm^2 V^{-1} s^{-1}$ with on−off ratios of about 1×10^4 under <10 V and PQT-12 TFTs had mobilities of 0.05−0.1 $cm^2V^{-1}s^{-1}$ with on−off ratios of about 1×10^3 to 1×10^4 under 3 V. This work provides a facile method for synthesis of high-k solution-processed perovskite nanoparticles-based dielectrics. This research also suggests that trapped state density at the semiconductor/dielectrics interface may be a critical factor to enable the low-voltage operation of organic TFTs.

Acknowledgment. This work is financially supported by Singapore A*STAR under Grant 052 117 0031.

Supporting Information Available: UV−vis, photoluminescence (PL), and energy dispersive spectrometer (EDS) spectra; organic TFT performance data (PDF). This material is available free of charge via the Internet at http://pubs.acs.org.